The Properties of Star-Forming Galaxies at z~2: Kinematics, Stellar Populations, and Metallicities

by

Dawn K. Erb

ISBN: 1-58112- 297-7

DISSERTATION.COM

Boca Raton, Florida
USA • 2005

The Properties of Star-Forming Galaxies at z~2:
Kinematics, Stellar Populations, and Metallicities

Dissertation.com
Boca Raton, Florida
USA • 2005

ISBN: 1-58112- 297-7

The Properties of Star-Forming Galaxies at $z \sim 2$: Kinematics, Stellar Populations, and Metallicities

Thesis by
Dawn K. Erb

In Partial Fulfillment of the Requirements
for the Degree of
Doctor of Philosophy

California Institute of Technology
Pasadena, California

2006

(Defended August 3, 2005)

Acknowledgements

More people than I can name here have helped to make the past five years happy and productive. My officemates at Caltech, Alison Farmer, Naveen Reddy, Jackie Kessler, and Alicia Soderberg, have always provided just the right amount of amusement and distraction. Patrick Shopbell, Anu Mahabal, and Cheryl Southard provided patient and knowledgeable technical support; and my especially heartfelt thanks to Patrick, Anu, Cheryl, and the makers of the DiskWarrior data recovery software, for saving me from having to repeat a significant amount of the work in this thesis. Thanks to P & L, and to Scott, Tatiana, Krista, Nancy, Alicia and my other teachers and friends at Yoga House, for always providing a welcoming, challenging and relaxing escape from the pressures of thesis-writing: namaste. Karin Menendez-Delmestre has been good company at home this last year. I have great appreciation for my collaborators in exploration of the $z \sim 2$ universe: Max Pettini, for being a great source of both encouragement and information, and for welcoming me on my visits to Cambridge; Kurt Adelberger, for always insightful comments and good though infrequent company; Naveen Reddy, for coming through all this with me from the beginning; and Alice Shapley, for her endless patience with my questions during the first years of this work, and for being a great observing partner on all those NIRSPEC runs. I hope there are more to come. And finally, I am especially grateful to have found one of the best advisors at Caltech in Chuck Steidel, who has always been encouraging, available, and patient with questions in spite of many other duties, and interested in any detail without ever losing sight of the big picture. He has always managed to strike just the right balance between showing concern with day to day operations and allowing independence. I am lucky to have collaborators who are such good people as well as good scientists. None of this would have happened without the support and encouragement of my parents, Dick and Judy Erb; the beginning of the belief that I could do this at all comes from them. And finally, to David Kaplan, for everything.

Abstract

We study the properties of star-forming galaxies at redshift $z \sim 2$, an era in which a substantial fraction of the stellar mass in the universe formed. Using 114 near-IR spectra of the Hα and [N II] emission lines and model spectral energy distributions fit to rest-frame UV through IR photometry, we examine the galaxies' star formation properties, dynamical masses and velocity dispersions, spatially resolved kinematics, outflow properties, and metallicities as a function of stellar mass and age. While the stellar masses of the galaxies in our sample vary by a factor of ~ 500, dynamical masses from Hα velocity dispersions and indirect estimates of gas masses imply that the variation of stellar mass is due as much to the evolution of the stellar population and the conversion of gas into stars as to intrinsic differences in the total masses of the galaxies. About 10% of the galaxies are apparently young starbursts with high gas fractions, caught just as they have begun to convert large amounts of gas into stars. Using the [N II]/Hα ratio of composite spectra to estimate the average oxygen abundance, we find a monotonic increase in metallicity with stellar mass. From the estimated gas fractions, we conclude that the observed mass-metallicity relation is primarily driven by the increase in metallicity as gas is converted to stars. The picture that emerges is of galaxies with a broad range in stellar population properties, from young galaxies with ages of a few tens of Myr, stellar masses $M_\star \sim 10^9$ M$_\odot$, and metallicities $Z \sim 1/3\, Z_\odot$, to massive objects with $M_\star \sim 10^{11}$ M$_\odot$, $Z \sim Z_\odot$, and ages as old as the universe allows. All, however, are rapidly star-forming, power galactic-scale outflows, and have masses in gas and stars of at least $\sim 10^{10}$ M$_\odot$, in keeping with their likely role as the progenitors of elliptical galaxies seen today.

Contents

List of Figures

List of Tables

Chapter 1

Introduction

Several lines of recent evidence indicate that the redshift range $1.5 \lesssim z \lesssim 2.5$ was one of the most active periods in the history of the universe. High levels of quasar activity and accretion onto massive black holes are indicated by the number density of luminous QSOs, which reaches a peak in this redshift range (e.g., Fan et al. 2001; Di Matteo et al. 2003), while the very bright but dusty submillimeter galaxies have recently been found to have a median redshift $z = 2.2$ (Chapman et al. 2005). Other studies indicate that much of the stellar mass in the universe today formed approximately during this redshift interval; Dickinson et al. (2003) find that 50–75% of the mass in today's galaxies had formed by $z \sim 1$, but only 3–14% had formed by $z \sim 2.7$. Similarly, Rudnick et al. (2003) find that the universe at $z \sim 3$ had $\sim 1/10$ the stellar mass density it has today, while half of the stellar mass in the universe had formed by $z \sim 1$–1.5. This era also sees the transition from the compact, irregular galaxies seen at $z \sim 3$ (Giavalisco et al. 1996) to the familiar Hubble sequence, which takes shape by $z \sim 1$.

Until recently, however, very little was known about the normal galaxies that populated the universe during this period. This span of cosmic time was known as the "redshift desert," because the strong emission lines usually used to identify galaxies shift out of the optical window past $z \sim 1.4$. However, such galaxies can in fact be selected efficiently by their rest-frame optical colors, through a method analogous to the selection of the Lyman break galaxies (LBGs) at $z \sim 3$. Their redshifts can be confirmed not through their optical emission lines, as has been traditional, but through their rest-frame UV spectra, which present a distinctive set of strong interstellar metal absorption lines. Advances in CCD sensitivity at short wavelengths have made such spectra relatively easy to obtain, as a typical $z \sim 2$ galaxy with $\mathcal{R} \sim 24$–25 can be well-detected with moderate $\sim$ 1–2 hour exposure times on a blue-sensitive multi-object spectrograph attached to an 8–10 m telescope. In this way we have assembled a sample of ~ 1000 galaxies with redshifts $1.5 \lesssim z \lesssim 2.6$. This thesis is concerned with the properties of these galaxies. We describe the selection of the sample, and the methods used to study the galaxies, in more detail below.

1.1 The Selection of Galaxies at $z \sim 2$

The selection criteria we use for the $z \sim 2$ galaxies are adapted from those used to identifiy the Lyman break galaxies at $z \sim 3$ (Steidel et al. 2003), which have distinctive colors in the $U_n G\mathcal{R}$ filter set as the Lyman break at 912 Å passes through the U_n filter. There is no comparable break with which to identify galaxies at $z \sim 2$, but nevertheless such objects occupy a unique region in the $U_n G\mathcal{R}$ plane. The color criteria used to select these galaxies were developed by using simple models to predict the colors that galaxies with SEDs similar to the LBGs would have at $z \sim 2$, and then empirically verified and adjusted to improve their efficiency. Overviews of the $z \sim 2$ selection techniques and spectroscopic sample are given by Adelberger et al. (2004) and Steidel et al. (2004), respectively. We show the $U_n G\mathcal{R}$ color selection window for galaxies with $2 \lesssim z \lesssim 2.5$ in the left panel of Figure 1.1 (from Adelberger et al. 2004), with

the predicted locations of galaxies at $z = 2$ and $z = 2.5$ shown by red and blue symbols. A histogram of the spectroscopic redshifts of galaxies selected by the $z \sim 2$ criteria is shown in the right panel. We use two sets of criteria aimed at galaxies with $1.5 \lesssim z \lesssim 2$ and $2 \lesssim z \lesssim 2.5$; most of our observing time has focused on candidates described by the higher redshift set. The surface density of objects satisfying either of the two criteria is ~ 9 arcmin^{-2}, and the fraction of low-redshift interlopers selected by the $2 \lesssim z \lesssim 2.5$ criteria is $\sim 9\%$, of which 3% are stars and 6% are star-forming galaxies at $z \sim 0.2$ (Steidel et al. 2004). Most interlopers are bright in the near-IR, with $K \lesssim 20$.

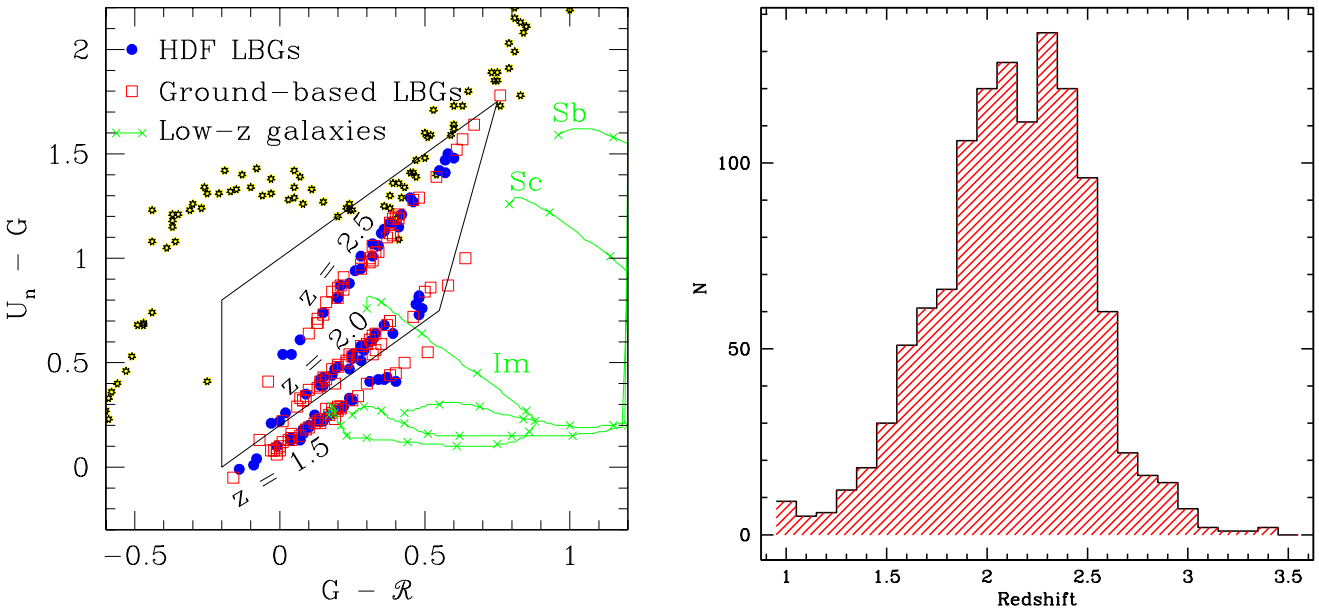

Figure 1.1 *Left:* The $U_n - G$ vs. $G - \mathcal{R}$ plane in which we select galaxies. The selection window for $2 \lesssim z \lesssim 2.5$ galaxies is shown by the trapezoid. It is primarily populated by star-forming galaxies in this redshift range, whose predicted locations (from de-redshifting the SEDs of the $z \sim 3$ LBGs) at $z = 2$ and $z = 2.5$ are shown by the red and blue symbols. A small fraction of interlopers, shown by stars (representing stars) and green tracks representing low-redshift galaxies, also enter the box. *Right:* A histogram of the spectroscopic redshifts of galaxies selected by the $z \sim 2$ critera. The distribution has $\langle z \rangle = 2.13 \pm 0.37$. 1198 galaxies are shown, 1031 of which have $1.5 < z < 2.6$.

No set of selection criteria will provide a complete sample, of course. It is not possible to use a single method to find all galaxies in a particular redshift range with reasonable efficiency; some balance must be struck between the fraction of interlopers allowed and the number of galaxies in the desired range rejected. Our $U_n G \mathcal{R}$ criteria miss all galaxies fainter than the $\mathcal{R} < 25.5$ cutoff; such objects may have very little current star formation or have nearly all their rest-frame UV light absorbed by dust. We also miss brighter highly reddened star-forming galaxies, which fall to the right of our selection window in Figure 1.1. Expanding the criteria to include these objects would substantially increase the interloper fraction as well.

Other criteria efficient at selecting galaxies at $z \sim 2$ have recently been developed. These are based on rest-frame optical colors, and are aimed at both star-forming (Daddi et al. 2004) and passive (Franx et al. 2003; Daddi et al. 2004) objects. Reddy et al. (2005) have recently quantified the overlap between the various samples, finding that galaxies selected by the $U_n G \mathcal{R}$ criteria account for $\sim 70\%$ of the star formation rate density at $z \sim 2$. The prime advantages of the rest-frame UV criteria are the modest amounts of observing time required (relative to the time needed to obtain deep K-band images for rest-frame optical

selection), and, especially, the focus on galaxies that are bright enough to examine spectroscopically. It is primarily from such spectra that we gain insights into their properties.

1.2 The Importance of Rest-Frame Optical Spectra

The bulk of this thesis concerns the interpretation of a large sample of rest-frame optical spectra of the $z \sim 2$ galaxies, primarily focused on the Hα emission line. For $2 \lesssim z \lesssim 2.5$, H$\alpha$ falls in the K-band, [O III] and Hβ in the H-band, and [O II] in the J-band. The measurement of the full set of lines for a large sample of objects requires a prohibitive amount of observing time, however, because most near-IR spectrographs can observe only one band at a time, and efficient multi-object near-IR spectrgraphs are still being developed. We have therefore concentrated on Hα, assembling a sample of 114 spectra.

Because it is produced in H II regions photoionized by massive stars, the Hα luminosity is directly related to the number of massive stars and is therefore commonly used as a diagnostic of the star formation rate (SFR). It is among the most well-calibrated of such indicators (e.g., Kennicutt 1998a; Charlot & Longhetti 2001; Brinchmann et al. 2004), and the dependence of the conversion between Hα luminosity and SFR on metallicity and other factors is relatively well-understood. For this reason observations of Hα are particularly valuable for determining the star formation properties of high redshift galaxies; such data minimize the systematic uncertainties involved in the comparisons of local and distant samples. Hα is arguably more useful than, for example, the rest-frame UV continuum, which is much more easily obtained for large samples at $z \gtrsim 2$ (requiring only optical photometry), because UV observations of local galaxies are more difficult.

Hα is also an extremely useful tracer of galaxies' kinematics. It is used to determine rotation curves locally and up to $z \sim 1$, and provides a measure of a galaxy's dynamical mass through the Hα velocity dispersion. Not surprisingly, the determination of the kinematic properties of high redshift galaxies presents fundamental problems not encountered in the local universe; the lack of a priori knowledge of the galaxies' structure, and the lack of spatial resolution in the spectra, mean that kinematic data, whether spatially resolved or not, are difficult to interpret. Thus observations of Hα in local starburst galaxies are particularly useful for our present purposes, as these systems are probably the closest analogs to the $z \sim 2$ galaxies in our sample. Such data at least suggest the extent to which Hα may trace the potential wells of starbursts (e.g., Lehnert & Heckman 1996), and at least one recent study of Hα in local starbursts directly addresses the issues likely to be encountered at high redshift (Colina et al. 2005).

Because they allow a determination of the systemic redshifts of distant galaxies, spectroscopic observations of Hα (or the other nebular emission lines) in combination with the rest-frame UV allow measurements of the outflow speeds of the galactic-scale winds that are ubiquitous in starburst galaxies at both low and high redshifts. Offsets of several hundred km s^{-1} are seen between the redshifts of the nebular lines and the interstellar absorption lines, which are typically blueshifted, and between the nebular lines and Lyα, which is redshifted (Pettini et al. 2001). These offsets are interpreted through the standard model in which we see interstellar absorption from approaching outflowing material, while Lyα is redshifted through resonant scattering off the receding shell on the far side of the galaxy. The outflow velocities of winds in local starbursts have been seen to vary with the masses and star formation rates of their host galaxies (Martin 2005; Rupke et al. 2005), and the determination of the outflow velocities in a large sample of $z \sim 2$ galaxies in combination with the SFRs and dynamical masses from Hα allow us to test for the existence of such correlations at high redshift.

Finally, the ratio of [N II]λ6583 to Hα correlates with the abunance of oxygen and is therefore useful as an indicator of metallicity (Pettini & Pagel 2004). Because the [N II] line is quite weak in individual spectra, composite spectra that increase the S/N are the only way to determine the abundances of all but the most metal-rich galaxies in our sample (for which [N II] can be well-detected in individual spectra;

Shapley et al. 2004). A large sample, which can be subdivided according to properties that might be expected to vary with metallicity, therefore enables useful studies of abundance trends at high redshift. We carry out such a study in Chapter 4, dividing the sample of Hα spectra into bins by both stellar mass and luminosity.

1.3 Stellar Population Parameters from Model Spectral Energy Distributions

The other major component of this thesis involves the estimation of the stellar masses, ages, star formation rates, and reddening of the $z \sim 2$ galaxies via the comparison of multi-wavelength photometry and model spectral energy distributions. Such techniques are well-established in the study of high redshift galaxies (Papovich et al. 2001; Shapley et al. 2001, 2005b). Photometry extending at least to the rest-frame optical (the observed K-band) is required, and the addition of rest-frame IR data, which are more senstive to older stars and somewhat less influenced by current star formation, improves the uncertainties considerably (Shapley et al. 2005b). Stellar masses are the most well-constrained of the fitted parameters, while degeneracies between age and reddening, which have a similar effect on the UV slope, limit the accuracy to which the other properties can be determined. For this reason the most useful results come from large samples; even when the properties of individual objects are uncertain, statistical trends can provide useful results. We focus here on relating the properties determined through SED modeling to those derived from the Hα spectra, looking particularly at variations of star formation rate, dynamical mass, and metallicity with stellar mass.

The outline of the thesis is as follows. Chapter 2 describes our pilot observations of Hα at $z \sim 2$, which were conducted in May 2002. We present results for 16 galaxies and focus on their kinematics and star formation rates. This chapter has been published as Erb et al. (2003). The work in Chapter 3 (published as Erb et al. 2004) was inspired by the surprisingly large fraction of galaxies in our pilot study that showed spatially resolved and tilted emission lines suggestive of rotation; it describes a study of the kinematics of galaxies selected for their elongated morphologies. In Chapter 4 we discuss the full sample of 114 spectra, and study the variations of the properties determined from Hα (including Hα line width and dynamical mass, amplitude of velocity shear, outflow velocities, Hα equivalent width, and star formation rate) with stellar mass, age and rest-frame optical luminosity. We also introduce estimates of the galaxies' gas masses, derived from the empirical local correlation between star formation density and gas density. In Chapter 5 we construct composite near-IR spectra as a function of stellar mass and find a relation between stellar mass and metallicity, which we examine in the context of the simple, "closed box" model of chemical evolution using the gas masses mentioned above. A brief epilogue describes two ways that new telescope instrumentation may enable the resolution of questions that remain from this work.

Chapter 2

Hα Spectroscopy of Galaxies at $z > 2$: Kinematics and Star Formation*†

Dawn K. Erb,[a] Alice E. Shapley,[a] Charles C. Steidel,[a‡] Max Pettini,[b]
Kurt L. Adelberger,[c§] Matthew P. Hunt,[a] Alan F. M. Moorwood,[d] & Jean-Gabriel Cuby[e]

[a]California Institute of Technology, Department of Astronomy, MS 105-24, Pasadena, CA 91125

[b]Institute of Astronomy, Madingley Road, Cambridge CB3 0HA, UK

[c]Harvard-Smithsonian Center for Astrophysics, 60 Garden Street, Cambridge, MA 02138

California Institute of Technology, Department of Astronomy, MS 105-24, Pasadena, CA 91125

[d]European Southern Observatory, Karl-Schwarzschild-Str. 2, D-85748 Garching, Germany

[e]European Southern Observatory, Alonso de Cordova 3107, Santiago, Chile

Abstract

We present near-infrared spectroscopy of Hα emission lines in a sample of 16 star-forming galaxies at redshifts $2.0 < z < 2.6$. Our targets are drawn from a large sample of galaxies photometrically selected and spectroscopically confirmed to lie in this redshift range. We have obtained this large sample with an extension of the broadband $U_nG\mathcal{R}$ color criteria used to identify Lyman break galaxies at $z \sim 3$. The primary selection criterion for IR spectroscopic observation was proximity to a QSO sightline; we therefore expect the galaxies presented here to be representative of the sample as a whole. Six of the galaxies exhibit spatially extended, tilted Hα emission lines; rotation curves for these objects reach mean velocities of ~ 150 km s^{-1} at radii of ~ 6 kpc, without corrections for inclination or any other observational effect. The velocities and radii give a mean dynamical mass of $\langle M \rangle \geq 4 \times 10^{10} M_\odot$. We have obtained archival *HST* images for two of these galaxies; they are morphologically irregular. One-dimensional velocity dispersions for the 16 galaxies range from ~ 50 to ~ 260 km s^{-1}, and in cases where we have both virial masses

*Based, in part, on data obtained at the W.M. Keck Observatory, which is operated as a scientific partnership among the California Institute of Technology, the University of California, and NASA, and was made possible by the generous financial support of the W.M. Keck Foundation. Also based in part on observations collected at the European Southern Observatory, Paranal, Chile (ESO Programme 66.A-0206).

†A version of this chapter was published in *The Astrophysical Journal*, vol. 591, 101–118.

‡Packard Fellow

§Harvard Society Junior Fellow

implied by the velocity dispersions and dynamical masses derived from the spatially extended emission lines, they are in rough agreement. We compare our kinematic results to similar measurements made at $z \sim 3$, and find that both the observed rotational velocities and velocity dispersions tend to be larger at $z \sim 2$ than at $z \sim 3$. We also calculate star formation rates (SFRs) from the Hα luminosities, and compare them with SFRs calculated from the UV continuum luminosity. We find a mean $\mathrm{SFR_{H\alpha}}$ of 16 $\mathrm{M_\odot\ yr^{-1}}$ and an average $\mathrm{SFR_{H\alpha}/SFR_{UV}}$ ratio of 2.4, without correcting for extinction. We see moderate evidence for an inverse correlation between the UV continuum luminosity and the ratio $\mathrm{SFR_{H\alpha}/SFR_{UV}}$, such as might be observed if the UV-faint galaxies suffered greater extinction. We discuss the effects of dust and star formation history on the SFRs, and conclude that extinction is the most likely explanation for the discrepancy between the two SFRs.

2.1 Introduction

Our knowledge of star-forming galaxies at high redshift has increased enormously in the past ten years, particularly at $z \sim 3$; large samples of galaxies at these redshifts are now known (Steidel et al. 1999, 2003), and they have been studied in both the rest-frame UV (Pettini et al. 2000; Shapley et al. 2003) and optical (Shapley et al. 2001; Papovich et al. 2001; Pettini et al. 2001), as well as at submillimeter (Chapman et al. 2000; Adelberger & Steidel 2000) and X-ray (Nandra et al. 2002) wavelengths to some extent. Much less is known about galaxies at $z \sim 2$. Because these objects lack strong spectroscopic features in the optical window, they have traditionally been difficult to identify. This is unfortunate, as $z \sim 2$ is likely the epoch in which a large fraction of the stars in the present day universe formed (Madau, Pozzetti, & Dickinson 1998; Blain et al. 1999), in which bright QSO activity reached its peak (Schmidt, Schneider, & Gunn 1995; Pei 1995; Fan et al. 2001), and in which rapidly star-forming galaxies of compact and disordered morphologies became the normal Hubble sequence galaxies of the $z < 1$ universe (Dickinson 2000).

The situation is improving, however. With the advent of sensitive IR detectors observations of rest-frame optical features are now feasible, and have been carried out successfully. Teplitz, Malkan, & McLean (1998) reported 11 Hα emitters discovered in a narrow-band IR imaging survey; Yan et al. (1999) and Hopkins, Connolly, & Szalay (2000) used slitless spectroscopy with the Near Infrared Camera and Multi-Object Spectrograph (NICMOS) on the *Hubble Space Telescope (HST)* to study the Hα luminosity function and star formation rate in galaxies at $z \leq 1.9$. Objects at $z \sim 2$ are in fact ideally suited for ground-based IR spectroscopy, since Hα falls in the K-band, [O III] and Hβ in the H-band, and [O II] in the J-band. This coincidence has been exploited with recent observations employing near-IR spectrographs on 8–10 m telescopes; most of these have focused on Hα emission (Kobulnicky & Koo 2000; Lemoine-Busserolle et al. 2003). Among these spectra is a rotation curve of a galaxy at $z \sim 2$ that reaches a velocity of $\gtrsim 200$ km s^{-1} (Lemoine-Busserolle et al. 2003), suggesting that near-IR spectroscopy may be able to provide the most detailed kinematic information yet available on galaxies at high redshift. It is also clear from most of the above results that star formation rates measured from Hα are consistently higher than those measured from the UV continuum luminosity; this is in accordance with observations at $z \sim 1$ (Glazebrook et al. 1999; Tresse et al. 2002) and at lower redshifts (e.g., Bell & Kennicutt 2001; also see Sullivan et al. (2000) and Buat et al. (2002) for comparisons of Hα and UV SFRs). The difference is generally accounted for by the differing sensitivities of the Hα and UV continuum star formation rate diagnostics to the presence of dust and to star formation history.

In this paper we present Hα spectroscopy in the K-band of 16 UV-selected galaxies in the redshift range $2.0 < z < 2.6$. In §2.2 we describe our target selection process, observations, and data reductions. In §2.3 we comment individually on any noteworthy features of the galaxies. Section 2.4 addresses the kinematics of the galaxies: we discuss the rotation curves in §2.4.1 and the one-dimensional velocity dispersions in §2.4.2. In §2.5 we calculate star formation rates from Hα and rest-frame UV emission and compare them,

and we discuss our conclusions in §2.6. We use a cosmology with $H_0 = 70$ km s^{-1} Mpc^{-1}, $\Omega_m = 0.3$, and $\Omega_\Lambda = 0.7$ throughout. In this cosmology, the universe at $z = 2.3$ is 2.8 Gyr old, or 21% of its present age, and a proper distance of 8.2 kpc subtends an angular distance of $1''$.

2.2 Target Selection and Observations

The objects discussed herein are drawn from a large sample of galaxies photometrically selected and spectroscopically confirmed to be in the redshift range $2.0 \leq z \leq 2.6$. We summarize the selection technique here; a more complete discussion will be given in a forthcoming paper. We have extended the broadband color criteria used to select galaxies at $z \sim 3$ (Steidel & Hamilton 1993; Steidel, Pettini, & Hamilton 1995; Steidel et al. 1996) to other regions of the $(U_n - G)$ vs. $(G - \mathcal{R})$ plane, identifying candidates according to the following conditions:

$$\begin{aligned} G - \mathcal{R} &\geq -0.1 \\ U_n - G &\geq G - \mathcal{R} + 0.2 \\ G - \mathcal{R} &\leq 0.3(U_n - G) + 0.2 \\ U_n - G &< G - \mathcal{R} + 1.0. \end{aligned} \tag{2.1}$$

We refer to these objects as "BX" (e.g., Q1700-BX691); 92% of the objects satisfying these criteria are galaxies in the redshift range $1.6 \leq z \leq 2.8$, with 72% in the range $2.0 \leq z \leq 2.6$. These criteria were developed by calculating the colors that typical $z \sim 3$ Lyman break galaxies (LBGs) would have if they were placed at $z \sim 2$; they are therefore designed to select objects with similar intrinsic spectral energy distributions (SEDs) at both redshifts (Adelberger 2002). Our sample also contains four "MD" objects (e.g., Q1623-MD107); these objects are detected in the U_n-band and meet the criteria

$$\begin{aligned} G - \mathcal{R} &< 1.2 \\ U_n - G &\leq G - \mathcal{R} + 1.5 \\ U_n - G &\geq G - \mathcal{R} + 1.0. \end{aligned} \tag{2.2}$$

They have the redshift distribution $\langle z \rangle = 2.79 \pm 0.27$ (Steidel et al. 2003), so that the low redshift end of the distribution encompasses objects with $z \leq 2.6$. Both the BX and MD candidates are restricted to $\mathcal{R} \leq 25.5$ (roughly equivalent to $\mathcal{R} \lesssim 26$ at $z \sim 3$). The two remaining objects in our sample, Q0201-B13 and CDFb-BN88, satisfy the BX criteria but have different names because they predated the systematic use of the $z \sim 2$ selection technique. Once candidates are photometrically identified, we confirm their redshifts with rest-frame UV spectra obtained with the Low Resolution Imaging Spectrometer (LRIS; Oke et al. 1995) on the Keck I telescope. The redshifts from the UV interstellar absorption lines and Lyα when present are listed in Table 2.1, and spectra for two of the objects are shown as examples in Figure 2.1. The rest-frame UV observations will be described in detail elsewhere.

The galaxies targeted for IR spectroscopy were selected as part of an ongoing project examining the interplay between galaxies and the intergalactic medium (IGM) in which we combine spectroscopy of faint star-forming galaxies with QSO absorption line observations of the IGM in the same volume (Adelberger et al. 2003). A detailed comparison of the galaxies and the IGM requires accurate measurements of the galaxy redshifts, and ultimately an understanding of the star formation rates, masses, and ages of galaxies near the QSO lines of sight; therefore the primary selection criterion (beyond the color criteria described above) for the present sample was proximity to a QSO sightline. This naturally results in a sample with a wide range of UV properties (as distinguished, for example, from the galaxies in the $z \sim 3$ sample of Pettini et al. (2001), which were selected to be particularly UV-bright).

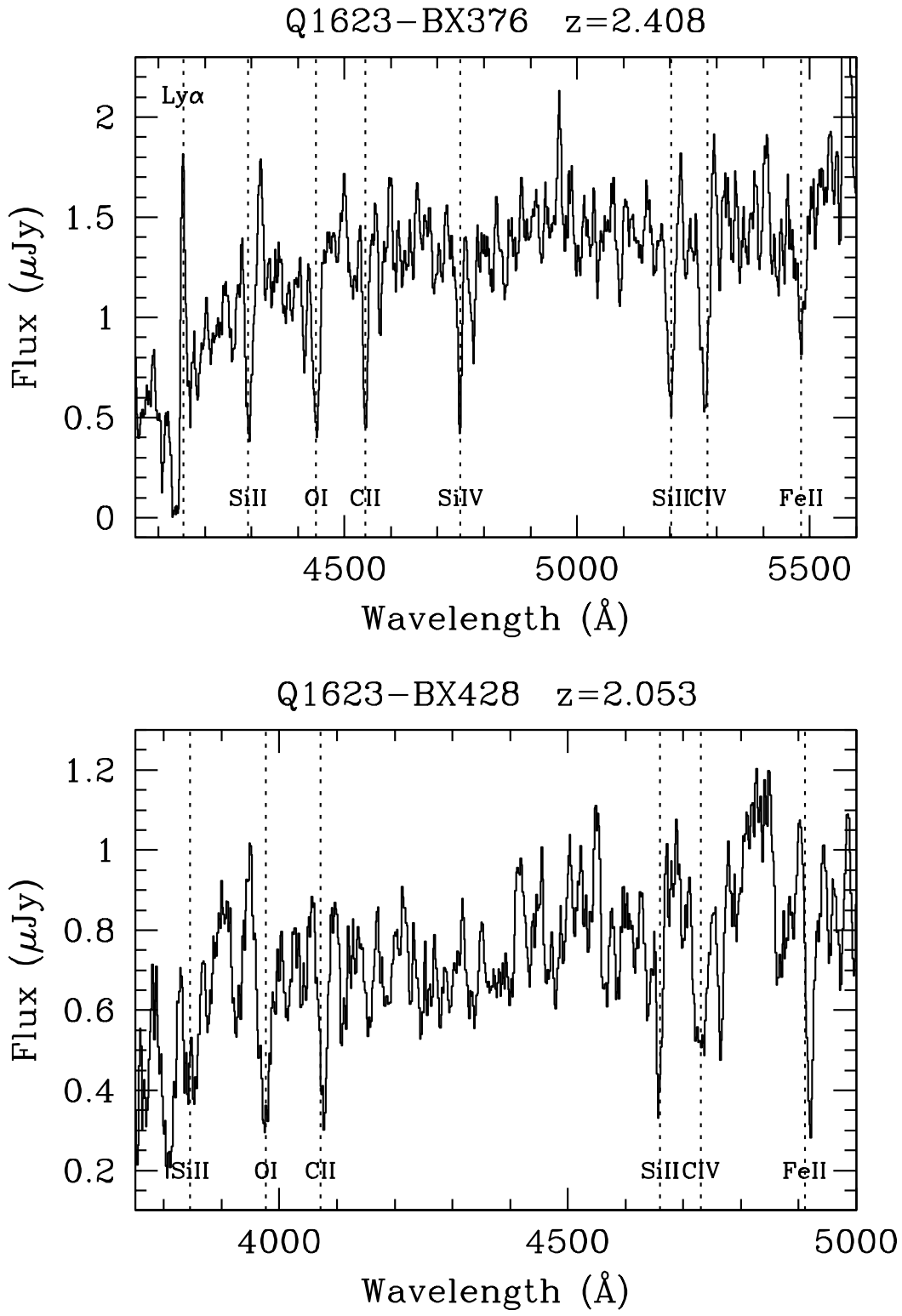

Figure 2.1 Sample rest-frame UV spectra for two of the galaxies. We show Q1623-BX376 at $z_{\rm abs} = 2.408$ (top), and Q1623-BX428 at $z_{\rm abs} = 2.053$ (bottom). The rest wavelengths of the lines labeled are Lyα λ1215 Å, SiII λ1260 Å, OI λ1302 Å, CII λ1334, SiIV λ1394, SiII λ1526, CIV λ1549, and FeII λ1608.

Twelve of our 16 galaxies are within 60″ of QSOs in fields at 1700+64 and 1623+27, and have redshifts slightly lower than those of the QSOs themselves; these were observed with the Near Infrared Imaging Spectrograph (NIRSPEC; McLean et al. 1998) on the Keck II telescope in May 2002. We observed an additional galaxy in the Groth-Westphal field on the same run. The other three objects in the sample (SSA22a-MD41, Q0201-B13, and CDFb-BN88) were observed with the Infrared Spectrometer and Array Camera (ISAAC; Moorwood et al. 1998) on the Very Large Telescope 1 (VLT 1) in October 2000, and were among the small number of $z \sim 2$–2.5 galaxies in the $z \sim 3$ LBG survey fields at the time. They were also selected because of their UV brightness, and because of the favorable wavelength of Hα relative to night sky emission lines and the possibility of measuring rotation.

2.2.1 Data Acquisition

Most of our targets were observed on May 19 and 20, 2002 (UT) with the NIRSPEC spectrograph on the Keck II telescope. NIRSPEC is described in detail by McLean et al. (1998); it uses a 1024 × 1024 pixel (ALADDIN2) InSb detector with 27 μm pixels. In the medium-dispersion mode used for these observations, each detector pixel corresponds to 0.″143 in the spatial direction, and the dispersion in the spectral direction is 4.2 Å per pixel. We used a 0.″76 × 42″ entrance slit, which gives a resolving power of $R \simeq 1400$ corresponding to a spectral resolution of ~ 15 Å FWHM in the observed frame K-band, as measured from the widths of sky lines. In almost all cases we were able to place two galaxies on the slit at the same time by setting the appropriate position angle. Because the galaxies are too faint to be acquired directly on the spectrograph slit, we placed them on the slit by offsetting from a nearby bright star or from the QSO with a sightline near the galaxy. Individual exposures were 900 s, and we typically took four exposures of each object for a total of 1 hour of integration. Between each exposure we reacquired the offset star, moved it along the slit by approximately 5″, and offset once again to the target object. The detector was read out in multiple-read mode, with 16 reads at the start and end of each integration; the results were then averaged to reduce noise. The choice of filter and wavelength range was governed by the expected position of the Hα line based on each galaxy's optical redshift; we used the NIRSPEC6 and NIRSPEC7 filters, which span the wavelength ranges 1.56–2.32 and 1.84–2.63 μm, respectively. The spectral dispersion allows a range of approximately 0.4 μm to be placed on the detector at one time. Conditions were photometric on both nights, with approximately 0.″5 FWHM seeing in K-band.

SSA22a-MD41, Q0201-B13, and CDFb-BN88 were observed on October 20–22, 2000 (UT) with the ISAAC spectrograph on the VLT1. The short-wavelength channel of ISAAC (Moorwood et al. 1998) uses a 1024 × 1024 pixel Rockwell HgCdTe array with 18.5 μm pixels. The pixel scale along the 1″× 120″ slit is similar to that of NIRSPEC, 0.″146 pixel^{-1}, but the spectral resolution is 2.5 times higher, with $R \simeq 3500$ and sky line widths of ~ 6 Å FWHM. We observed in the K-band, again targeting the expected position of Hα from rest-frame UV redshifts. The position angles were chosen to align with the major axes of the galaxies if any extended structure was apparent in the optical images; this was the case with SSA22a-MD41 and with CDFb-BN88 to a lesser extent. We also placed a bright star on the slit along with each galaxy to facilitate the determination of offsets between images. We performed an ABBA series of four 720 second exposures, with 10″ offsets between the A and B positions. The object was then reacquired at a different position along the slit and the procedure was repeated, typically for a total of ~ 3 hours of integration. Conditions were not photometric, and the seeing varied between 0.″5 and 0.″6 FWHM. The targets and observations are summarized in Table 2.1.

2.2.2 Data Reduction

The fully reduced spectra are shown in Figure 2.2. The two-dimensional images were reduced with IRAF; preliminary steps included flagging and masking any pixels that exhibited aberrant behavior in the dark